1-1-2000

Effects of Nozzle-Inlet Chamfering on Pressure Drop and Heat Transfer in Confined Air Jet Impingement

L. A. Brignoni

S V. Garimella
Purdue Univ, sureshg@purdue.edu

PERGAMON

International Journal of Heat and Mass Transfer 43 (2000) 1133–1139

International Journal of HEAT and MASS TRANSFER

www.elsevier.com/locate/ijhmt

Effects of nozzle-inlet chamfering on pressure drop and heat transfer in confined air jet impingement

Luis A. Brignoni, Suresh V. Garimella*

Department of Mechanical Engineering, University of Wisconsin-Milwaukee, P.O. Box 784, Milwaukee, WI 53201, USA

Received 15 January 1999; received in revised form 8 June 1999

Abstract

The effect of changing the nozzle geometry on the pressure drop and local heat transfer distribution in confined air jet impingement on a small heat source was experimentally investigated. Heat transfer and pressure drop measurements obtained with chamfered nozzles were compared to those obtained with a square-edged (non-chamfered) nozzle of the same diameter for different turbulent Reynolds numbers in the range of 5000–20,000, nozzle-to-target spacings, chamfer angles and chamfer lengths. The ratio of average heat transfer coefficient to pressure drop was enhanced by as much as 30.8% as a result of chamfering the nozzle, with narrow chamfering providing the better performance.

1. Introduction

Impinging jets have been widely used for applications where high heat and mass transfer rates are required. A variety of nozzle geometries ranging from slots to square-edged orifices and converging and diverging round nozzles have been studied. For the submerged and confined impinging jets considered here, the radial outflow is confined in a narrow channel bounded by the target surface and the plate containing the nozzle; the effect of confinement is generally to degrade heat transfer. Previous studies [1,2] have investigated the dependence of heat transfer on parameters such as Reynolds number ($U_j d/v$), nozzle-to-target spacing (H/d), and nozzle diameter (d). Nozzle geometry parameters such as nozzle diameter and length (l) as well as the orifice inlet and exit shapes have been found to play a determining role in heat transfer [3–7]. Heat transfer coefficients were found to be highest for small values of l/d. Square-edged orifices were found to have turbulence levels higher than for contoured nozzles [6,7] resulting in higher heat transfer coefficients. The orifice design in jet impingement is also important because it affects the pressure drop across the nozzle and the velocity profiles along the target surface; as a result, the heat transfer rates are affected [4].

The present study aims to experimentally investigate the effect of changing the nozzle geometry from square-edged to chamfered on the pressure drop and local heat transfer distribution in confined axisymmetric air jet impingement. In contrast to the contoured [5] and hyperbolic [4] nozzles previously studied, chamfering the nozzle inlets requires a very simple machining operation (e.g., counter-sinking), which was the consideration that motivated the present study. The experimental parameters include nozzle

* Corresponding author. Present address: School of Mechanical Engineering, Purdue University, West Lafayette, IN 47907, USA. Tel.: +1-765-494-5621; fax: +1-765-494-0539.

E-mail address: sureshg@ecn.purdue.edu (S.V. Garimella).

0017-9310/00/$ - see front matter
PII: S0017-9310(99)00207-0

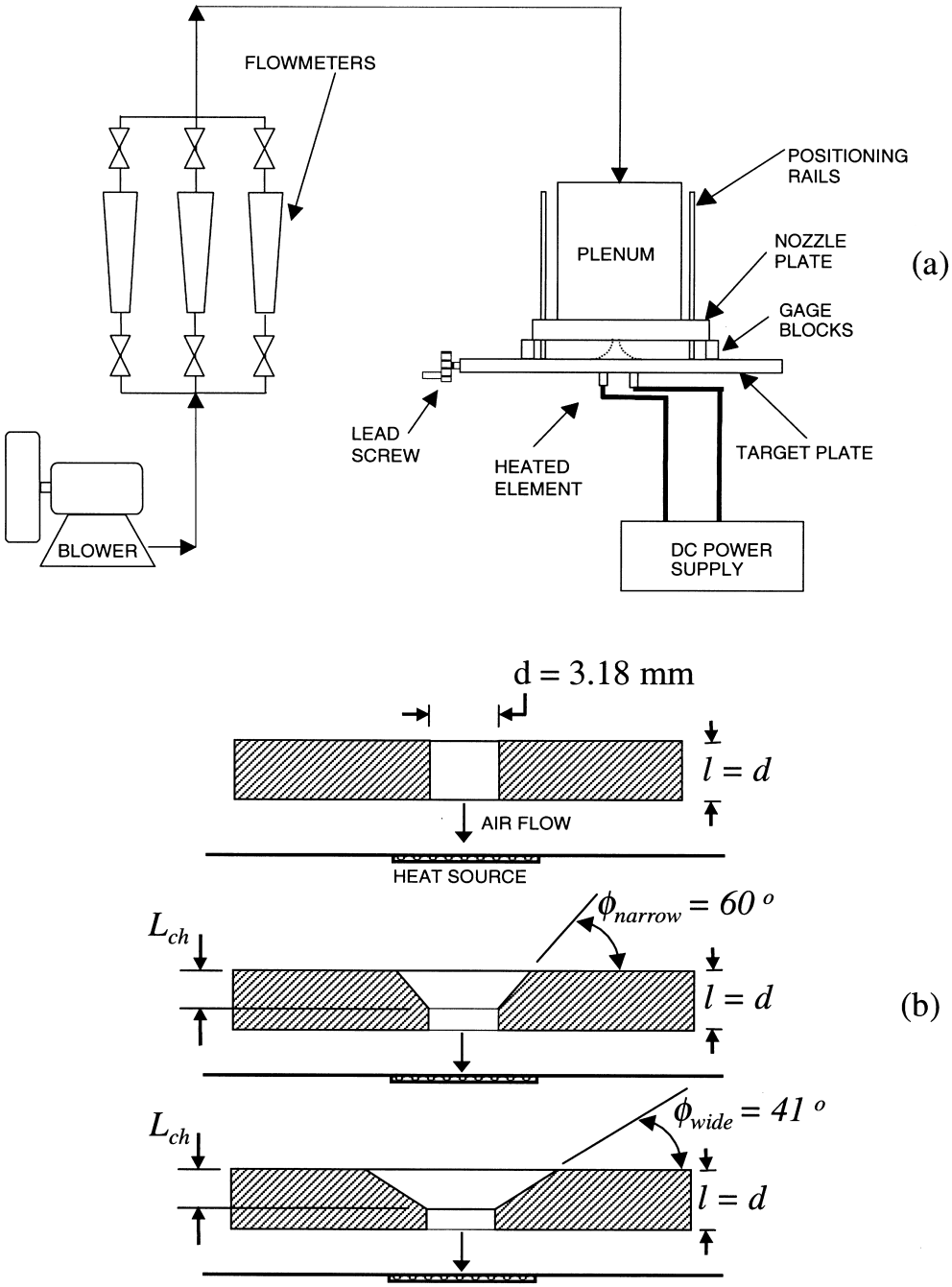

Fig. 1. (a) Schematic of the air jet impingement facility. (b) Section view of the nozzle geometries tested (three values of chamfer depth for each chamfer angle).

chamfer angle ϕ, chamfer depth L_{ch}, Reynolds number Re, and nozzle-to-target spacing. The specific goal of this work is to identify conditions under which pressure drop across the nozzle may be reduced without significantly altering the heat transfer rate, or equivalently, to enhance heat transfer while keeping the pressure drop constant. At a fixed flow rate, a reduction in pressure drop amounts to a proportional reduction in the pumping power required to drive the flow. Local measurements of the heat transfer coefficient are presented as a function of H/d, Re, ϕ, and L_{ch}. Heat transfer and pressure drop measurements

obtained with the chamfered nozzles are compared to those obtained with a square-edged (non-chamfered) nozzle of the same diameter.

2. Experiments

The air jet impingement facility (Fig. 1(a)) used in the experiments is the same as that used by Schroeder and Garimella [1,2], and only important details are provided here. Air flow rate is measured by one of three flowmeters mounted in parallel, depending on the range. Several valves in conjunction with a variable-speed drive controller help to set the required flow rate. The air is delivered to a flow-conditioning cylindrical plenum in the test section. Interchangeable nozzle plates are attached to the lower end of the plenum; the nozzle plate serves to confine the flow to being nominally radial after impingement. The static pressure in the plenum is measured using a pressure tap located in the wall connected to a manometer. The nozzle-to-target spacing is set using three high-precision gage blocks. Two spacings were employed for the experiments, $H/d = 1$ and 4. The temperature of the air jet was measured using a 36 gauge T-type thermocouple located just prior to the plenum exit.

The orifice diameter was held at $d = 3.18$ mm for all the experiments. The orifice geometry for the nozzle plates used is shown in Fig. 1(b). Two sets of nozzle plates with two different chamfer angles were tested: a *narrow* chamfer with an angle $\phi = 60^\circ$ and a *wide* chamfer with $\phi = 41^\circ$. Values of chamfer depth tested with each chamfer angle were $L_{ch} = 0.64$, 1.47, and 2.31 mm. A square-edged orifice ($l/d = 1$) was also considered in order to provide a baseline for the experiments. The aspect ratio l/d used was held equal to unity for all the nozzle plates; this was achieved by machining the nozzle plate thickness to be equal to the nozzle diameter ($l = d = 3.18$). Local and average heat transfer coefficients were measured at two Reynolds numbers of 5000 and 20,000 for the three plates at $H/d = 1$ and 4. Pressure drop measurements were obtained for $H/d = 1$ and 4 for a range of Reynolds numbers ($5000 < Re < 25{,}000$, in increments of 5000).

The heat source consists of a stainless steel foil (0.0762 mm thick) with a heated area of 20×20 mm^2, flush mounted to, and insulated from, the target plate. A 36 gauge T-type thermocouple located on the underside at the center of the stainless steel foil measures the local temperature distribution of the heated surface as the heat source assembly is traversed with respect to the jet in minimum increments of 0.5 mm. This technique of measuring local heat transfer coefficients is discussed in detail elsewhere [1,2,8]. It is emphasized that since the traversal of the heat source with respect to the impinging jet is limited to the extent of the heated area (stagnation point always positioned on the heater), the thermal boundary layer development is not altered as the heat source is moved relative to the jet. The voltage drop across the heater was measured directly; the current was determined from the voltage drop across a calibrated resistance shunt mounted in series with the circuit. The heat generation was determined as a product of the measured voltage and current. The power input was adjusted so that the average temperature difference between the air jet and the heated surface was approximately 15°C. Temperature readings from thermocouples located at the top and bottom of the insulation layer underneath the foil showed the power loss by conduction to be typically 4% of the heat generation. Radiation losses were estimated to be less than 1% of the generated power [9]. The conduction and radiation losses were incorporated into the data reduction program and subtracted from the heat generation in each experiment.

The local heat transfer coefficients were determined as

$$h = \frac{q_{out}}{A_h(T_s - T_j)} \tag{1}$$

where q_{out} is the convected heat, A_h is the area of the heater, T_s is the local surface temperature, and T_j is the air jet temperature. The data from each experiment were also area-averaged over the square heat source to obtain an average heat transfer coefficient,

$$\bar{h} = \frac{q_{out}}{\sum[A_i(T_{si} - T_j)]} \tag{2}$$

where T_{si} is the local surface temperature measured for the annular band of area A_i straddling the location of each temperature measurement; at the corners of the heat source, the annuli are fragmented. Additional details of the heat source construction and heat transfer calculations are available in [8,9].

The uncertainty in measured heat transfer coefficients at 95% confidence was estimated to be less than 4.5%. The largest contribution to the uncertainty comes from the temperature measurement (± 0.3°C). The uncertainty in pressure drop lies in reading error and was estimated to be less than 4.2%.

3. Results and discussion

The local heat transfer coefficient distributions for the three chamfer angles (41°, 60°, and unchamfered) are shown in Figs. 2 and 3, respectively for two of the three chamfer depths studied ($L_{ch} = 0.64$ and 2.31 mm). In each figure, two Reynolds numbers ($Re = 5000$, 20,000) and two nozzle-to-target spacings

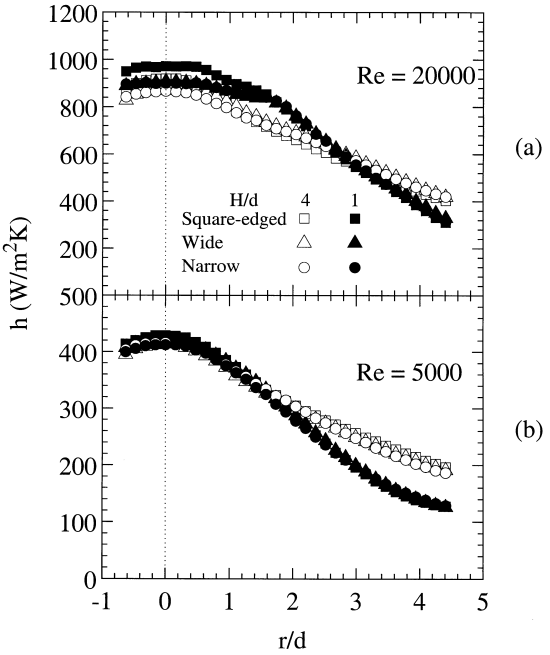

Fig. 2. Local heat transfer coefficient distribution at shallow chamfer depth ($L_{ch} = 0.64$ mm) for (a) $Re = 20{,}000$ and (b) $Re = 5000$.

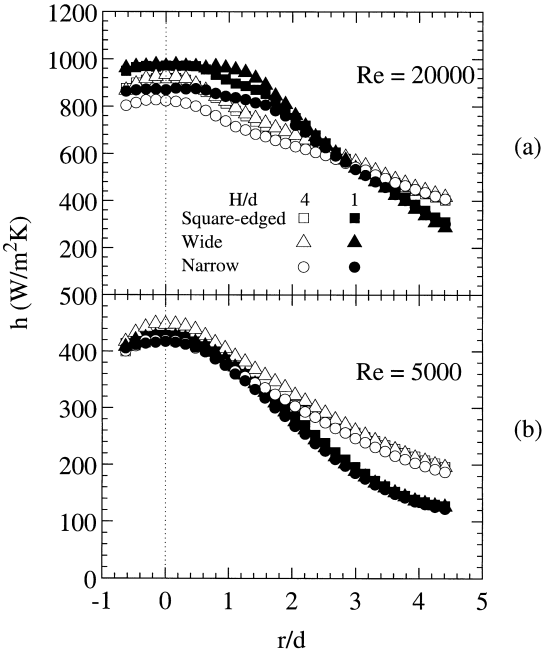

Fig. 3. Local heat transfer coefficient distribution at large chamfer depth ($L_{ch} = 2.31$ mm) for (a) $Re = 20{,}000$ and (b) $Re = 5000$.

($H/d = 1$, 4) are considered. The local heat transfer coefficients for $r/d > 2$ show a monotonic decrease and are very similar for the three chamfer angles under comparable conditions (same H/d and Re) in both figures. At $Re = 20{,}000$ and $H/d = 1$, Figs. 2 and 3 ($L_{ch} = 0.64$ and 2.31 mm, respectively) show similar trends in the local heat transfer coefficients for the square-edged nozzle and the two chamfered nozzles, including the existence of mild secondary peaks. The secondary peaks have been attributed to a transition to turbulence along the radial outflow. In confined impingement configurations as in the present study, the peaks may also be due to reattachment of the toroidal recirculating flow pattern. Fig. 3 shows that heat transfer coefficients are slightly higher with the wide chamfer nozzle at $Re = 5000$ and $H/d = 4$ in the range $0 < r/d < 3$. Fig. 3 also shows that for $Re = 20{,}000$ and $H/d = 1$ the secondary peak obtained with the wide chamfer nozzle is more pronounced, resulting in a higher average heat transfer coefficient.

For chamfer depths $L_{ch} = 0.64$ and 1.47 mm (latter not shown) the square-edged (unchamfered) nozzle shows slightly higher stagnation heat transfer coefficients ($r/d \sim 0$) at $H/d = 1$ (see Fig. 2). This is also true at $H/d = 4$, although the effect is less distinct. For a chamfer depth of 2.31 mm the highest stagnation heat transfer coefficient was obtained with the wide chamfer nozzle at $Re = 5000$ and $H/d = 4$ (Fig. 3). However, for the same chamfer depth at $Re = 20{,}000$, the wide chamfered nozzle and the square-edged nozzle have very similar values for stagnation heat transfer coefficients.

Table 1 shows the pressure drop measurements for all the flow rates and nozzle geometries considered. Table 2 shows the corresponding average heat transfer coefficients obtained; only two flow rates were considered in the heat transfer tests. The results obtained with the two chamfer angles may be compared from these tables under similar flow conditions against those obtained with the square-edged orifice. For example, the greatest pressure drop reduction by changing the nozzle geometry from square-edged to chamfered is by 24.1% for $Re = 20{,}000$, $H/d = 4$, with the narrow chamfer at the maximum chamfer depth tested ($L_{ch} = 2.31$ mm). Table 2 shows that under these conditions, the average heat transfer coefficient is reduced by only 2.7%. As another example, the greatest reduction in average heat transfer coefficient of 4.7% (narrow chamfer, $Re = 5000$, $H/d = 1$, $L_{ch} = 2.31$ mm) is accompanied by a decrease in pressure drop of 17.7%. Tables 1 and 2 show that the narrow chamfer results in decreases in pressure drops in all cases at the expense of only small changes in $\bar{h}$.

With the wide chamfer, pressure drop reductions are obtained for chamfer depths of 0.64 and 1.47 mm, the maximum reduction for this nozzle being by 22.5% for $Re = 20{,}000$, $H/d = 4$, and $L_{ch} = 1.47$ mm. The corresponding change in $\bar{h}$ is negligible (0.12%). Further

Table 1
Pressure drop measurements for all conditions tested; the nozzle studied was 3.18 mm in diameter

Re	$\Delta P_{\text{square-edged}}$ (kPa)		ϕ	$\Delta P_{0.64\text{ mm}}$ (kPa)		$\Delta P_{1.47\text{ mm}}$ (kPa)		$\Delta P_{2.31\text{ mm}}$ (kPa)	
	$H/d=4$	$H/d=1$		$H/d=4$	$H/d=1$	$H/d=4$	$H/d=1$	$H/d=4$	$H/d=1$
5000	0.58	0.56	Wide chamfer	0.52	0.52	0.53	0.51	0.63	0.61
10,000	1.80	1.77		1.56	1.53	1.63	1.58	1.96	1.93
15,000	4.09	3.72		3.42	3.38	3.08	3.05	4.40	4.16
20,000	6.60	6.26		5.58	5.68	5.11	5.07	7.27	7.24
25,000	9.98	8.96		8.46	8.29	7.61	7.44	10.15	10.11
5000	0.58	0.56	Narrow chamfer	0.50	0.48	0.49	0.47	0.51	0.50
10,000	1.80	1.77		1.51	1.48	1.62	1.58	1.67	1.63
15,000	4.09	3.72		3.21	3.05	3.14	3.05	3.21	3.14
20,000	6.60	6.26		5.41	5.41	5.07	5.04	5.01	4.90
25,000	9.98	8.96		8.42	7.85	7.41	7.27	6.93	6.87

increases in chamfer depth, however, were found to cause an increase in pressure drop. For example, at $Re = 20{,}000$ and $H/d = 1$, increasing the length of the wide chamfer to $L_{ch} = 2.31$ mm causes an increase in pressure drop by 15.7% when compared to the square-edged nozzle. This increase in pressure drop is accompanied by a slight decrease in $\bar{h}$ of 0.7%.

Lowering the nozzle-to-target spacing produces modest reductions in pressure drop for all nozzles tested while the heat transfer coefficients were affected to a larger extent. The greatest reduction in ΔP of 10.2% obtained by decreasing H/d from 4 to 1 is with the square-edged nozzle at $Re = 25{,}000$. Amongst the chamfered nozzles, the narrow chamfer offers the greatest reduction in pressure drop of 6.8% ($Re = 25{,}000$, $L_{ch} = 0.64$ mm) when H/d is decreased. Figs. 2 and 3 show that for a given Reynolds number a change in nozzle-to-target spacing produces perceptible changes in local heat transfer coefficients. While reductions in $\bar{h}$ of roughly 20% ($L_{ch} = 2.31$ mm) result when H/d is decreased from 4 to 1 at $Re = 5000$, $\bar{h}$ increases slightly or remains unchanged with changes in H/d at $Re = 20{,}000$.

Possible mechanisms for the observed effects of chamfer geometry may be deduced as follows. It is observed that for a chamfer angle of 60° (narrow), the pressure drop is significantly lower than for the square-edged counterpart. This decrease in pressure drop may be attributed to the removal of the sharp corner at the inlet leading to an alleviation of the vena contract within the nozzle, and the associated reduction in pressure losses. However, as the chamfer angle is decreased to 41° (wide), this salutary effect of decreasing pressure losses is less evident, and the pressure drop increases again. In the limit, as the chamfer angle approaches zero, the nozzle effectively reverts to becoming square-edged once again, with no chamfer — the same limit is encountered as the chamfer angle is increased to 90°. As these limits of very wide or very narrow chamfering are approached, the pressure drop incurred would be the same as for an unchamfered nozzle. This suggests that an intermediate chamfer angle would provide the greatest reduction in pressure drop. Although only two intermediate values were tested in the present study, it appears that the optimal chamfer angle is closer to 60°. As for the effect of chamfer depth, as L_{ch} increases, the pressure drop is seen to reduce to a certain point and then increase

Table 2
Average heat transfer coefficients obtained with the nozzles tested (square-edged, wide chamfer, and narrow chamfer)

Re	$\bar{h}_{\text{square-edged}}$ (W/m^2 K)		ϕ	$\bar{h}_{0.64}$ (W/m^2 K)		$\bar{h}_{1.47}$ (W/m^2 K)		$\bar{h}_{2.31}$ (W/m^2 K)	
	$H/d=4$	$H/d=1$		$H/d=4$	$H/d=1$	$H/d=4$	$H/d=1$	$H/d=4$	$H/d=1$
5000	282	230	Wide chamfer	275	233	286	227	291	227
20,000	602	623		632	630	602	620	619	619
5000			Narrow chamfer	275	230	276	238	274	219
20,000				622	626	605	618	586	601

again. The loss coefficient for chamfered nozzles [10] decreases with increasing L_{ch} to a certain point. For instance, as L_{ch} increases from 0.025 to 0.6d, the loss coefficient for the narrow chamfer angle (60°) decreases from 0.4 to 0.12, whereas for the wide chamfer angle (41°), the loss coefficient decreases from 0.42 to only 0.23. The observed trend towards higher pressure drop for the wider chamfer angle is consistent with the larger loss coefficients for this chamfer angle. The reduction in loss coefficient with increasing L_{ch} in this range (at a fixed mass flow rate) implies a decrease in pressure drop, and may explain the reason for the decrease in pressure drop as L_{ch} goes from 0.64 to 1.47 mm. It is not clear why the pressure drop increases for further increases in L_{ch}; no loss coefficient data are available in [10] for the largest chamfer depth studied.

The objective of this study was to reduce pressure drop without compromising the thermal performance of the nozzles studied. For square-edged nozzles, a reduction in pressure drop for a given pumping power implies a drop in flow rate and is accompanied by a reduction in the average heat transfer coefficient [1,2]. However, at a given flow rate, changing the nozzle geometry from square-edged to chamfered provides a reduction in pressure drop without significantly altering the heat transfer. A performance parameter which accounts for the combined changes in heat transfer and pressure drop is $\bar{h}/\Delta P$. To facilitate a comparison of the performance of square-edged and chamfered nozzles, Fig. 4 shows the percent enhancement in $\bar{h}/\Delta P$ for the chamfered nozzles relative to the square-edged nozzle, as a function of chamfer depth L_{ch}. In all cases except for the wide chamfer at the largest chamfer depth, chamfering is seen to provide an enhancement in $\bar{h}/\Delta P$. The intermediate chamfer depth is seen to provide an optimum enhancement level. The maximum enhancement in $\bar{h}/\Delta P$ of 30% is obtained for the intermediate chamfer depth with either chamfer angle. At the wide chamfer angle and the largest chamfer depth, a degradation of performance below that of the square-edged nozzle is seen. In general, higher $\bar{h}/\Delta P$ enhancement levels are obtained for the narrow chamfer angle at the larger nozzle-to-target spacing and larger Reynolds number.

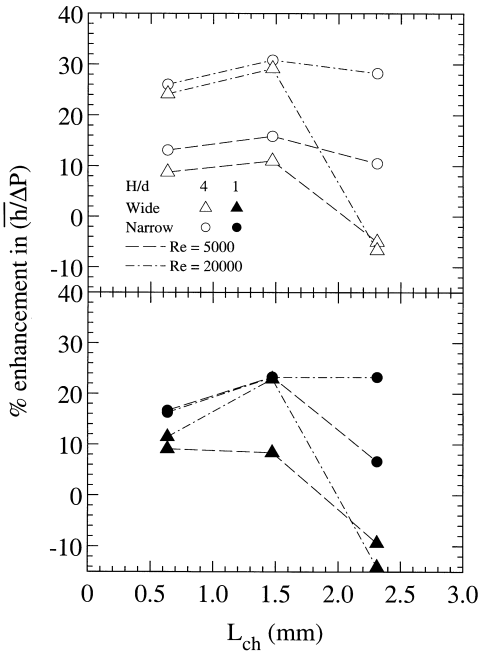

Fig. 4. Percentage enhancement due to chamfering of the ratio of average heat transfer coefficient to pressure drop as a function of chamfer depth for $H/d = 1$ and 4.

4. Conclusion

Compared to square-edged nozzles, chamfering the nozzle inlet produces significant reductions in pressure drop; the average heat transfer coefficient, on the other hand, is not strongly affected. Inlet chamfering may also be achieved with a relatively simple fabrication step for implementation of jet impingement in practical designs. In general, narrow chamfering was more effective in terms of reducing the pressure drop when compared to the wide chamfer nozzle performance. Enhancements in the performance parameter $\bar{h}/\Delta P$ of up to 30.8% were obtained in this study as a result of chamfering the nozzle inlet, relative to unchamfered nozzles.

Acknowledgements

Partial funding for this work provided by Cray Research of Chippewa Falls, Wisconsin is gratefully acknowledged. LAB was supported through a UWM AOP Fellowship.

References

[1] V.P. Schroeder, S.V. Garimella, Heat transfer from a discrete heat source in confined air jet impingement, Heat Transfer 5 (1998) 451–456.
[2] V.P. Schroeder, S.V. Garimella, Heat transfer in the confined impingement of multiple air jets, Procs. ASME Heat Transfer Division 361 (1) (1998) 183–190.
[3] S.V. Garimella, B. Nenaydykh, Nozzle-geometry effects in liquid jet impingement heat transfer, International Journal of Heat and Mass Transfer 39 (1996) 2915–2923.
[4] D.W. Colucci, R. Viskanta, Effect of nozzle geometry on local convective heat transfer to a confined imping-

ing air jet, Experimental Thermal and Fluid Science 13 (1996) 71–80.

[5] N.T. Obot, A.S. Majumdar, W.J.M. Douglas, The effect of nozzle geometry on impingement heat transfer under a round turbulent jet, ASME Paper No. 79-WA/HT-53, ASME, New York, 1979.

[6] J. Stevens, Y. Pan, B.W. Webb, Effect of nozzle configuration on transport in the stagnation zone of axisymmetric, impinging free-surface liquid jets. Part 1: turbulent flow structure, Journal of Heat Transfer 114 (1992) 874–879.

[7] Y. Pan, J. Stevens, B.W. Webb, Effect of nozzle configuration on transport in the stagnation zone of axisymmetric, impinging free-surface liquid jets. Part 2: local heat transfer, Journal of Heat Transfer 114 (1992) 880–886.

[8] S.V. Garimella, R.A. Rice, Confined and submerged liquid jet impingement heat transfer, Journal of Heat Transfer 117 (1995) 871–877.

[9] V.P. Schroeder, Heat transfer from a discrete heat source in confined air jet impingement with single and multiple orifices, M.S. thesis, University of Wisconsin, Milwaukee, 1997.

[10] R.D. Blevins, Applied Fluid Dynamics Handbook, Krieger, New York, 1992, p. 74.